A Nonlocal Total Variation Model for Image Decomposition: Illumination and Reflectance

Wei Wang[1] and Michael K. Ng[2,*]

[1] *Department of Mathematics, Tongji University, Shanghai, China.*
[2] *Department of Mathematics, Hong Kong Baptist University, Kowloon Tong, Hong Kong.*

Abstract. In this paper, we study to use nonlocal bounded variation (NLBV) techniques to decompose an image intensity into the illumination and reflectance components. By considering spatial smoothness of the illumination component and nonlocal total variation (NLTV) of the reflectance component in the decomposition framework, an energy functional is constructed. We establish the theoretical results of the space of NLBV functions such as lower semicontinuity, approximation and compactness. These essential properties of NLBV functions are important tools to show the existence of solution of the proposed energy functional. Experimental results on both grey-level and color images are shown to illustrate the usefulness of the nonlocal total variation image decomposition model, and demonstrate the performance of the proposed method is better than the other testing methods.

1. Introduction

In this paper, we address the problem of decomposing an image into its illumination and reflectance components. The illumination component is modeled as the amount of light intensity onto the objects in the image scene. The reflectance component is related to the light source reflected based on the nature of the objects in the image scene. There are many applications of such image decomposition like image enhancement and shadow removal, see [1–5].

---

*Corresponding author. *Email addresses:* `wangw@tongji.edu.cn` (W. Wang), `mng@math.hkbu.edu.hk` (M. K. Ng)

The recovery of the illumination and reflectance components from a given image is known to be an ill-posed problem [6, 7]. Land and McCann's Retinex algorithm [6, 8, 9] successfully decompose an image into the illumination and reflectance components. The Retinex algorithm is based on random walk and is a path-based algorithm. In [10–13], the researchers further proposed to develop recursive algorithms via recursive matrix operations to perform image decomposition into illumination and reflectance components. The efficiency of recursive algorithms is better than that of the path-based methods. Recently, several variational frameworks for Retinex theory are studied [1–5, 14–24]. In the setting, a mathematical optimization problem is formulated by decomposing an input image into the reflectance and illumination components, where their pointwise multiplication between these two components is assumed to be given input image. In [5], Kimmel et al. assumed that the illumination component was smooth and employed such smoothness condition in the objective function. In [20], bilateral filters were also used to construct regularization terms to perform image decomposition. In [3, 4, 15–19], the illumination component was assumed to be smooth and the reflectance component was assumed to be a piecewise constant function. According to these two assumption, a Poisson equation was set up for image decomposition. In [21], Ma and Osher proposed to use total variation and nonlocal total variation regularization models for Retinex theory. In their method, Bregman iteration was used to solve their models. In [22], Ma et al. further proposed a L_1-based variational model which is focused on recovering the reflectance component. In [23], Zosso presented a unifying framework for Retinex theory that is able to study many of the existing Retinex implementations including the methods in [21] and [22]. In [24], Ng and Wang developed and studied a total variation model for image decomposition which considers both reflectance and illumination components in the objective function.

The main aim of this paper is to use nonlocal bounded variation (NLBV) techniques to decompose an image intensity into the illumination and reflectance components. By considering spatial smoothness of the illumination component and nonlocal total variation (NLTV) of the reflectance component in the decomposition framework, an energy functional is constructed. The motivation behind is that the reflectance component contains a sparse set of texture patches in the space of nonlocal bounded variation functions. As an example, we compare in Fig. 1 the image decomposition of using the NLTV model and that of using the TV model [24]. We see from the figure that the reflectance component by the NTLV model (especially the upper region) is visually sharper and clearer than that by the TV model[†].

There are two main contributions in this paper. Firstly, we establish the theoretical results of the space of NLBV functions such as lower semicontinuity, approximation and compactness. These essential properties of NLBV functions are important tools to show the existence of solution of the proposed energy functional. To the best of our

---

[†]Here we have used the best set of parameters chosen in [24] for the TV image decomposition model ($c_1 = 1$, $c_2 = 0.1$ and $c_3 = 10^{-5}$), and the best set of parameters for the NLTV model ($c_1 = 1$, $c_2 = 1$ and $c_3 = 10^{-5}$).
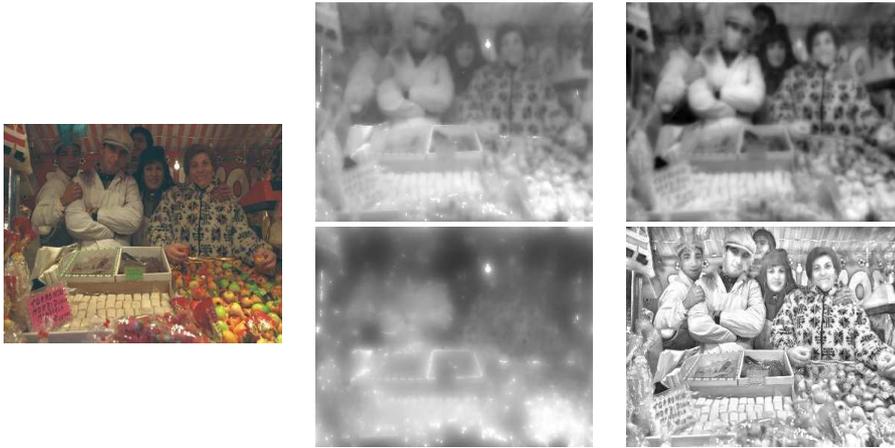
Figure 1: The first column: the input image; the second column: the illumination component by using TV (upper) and NLTV (lower) models; the third column: the reflectance component by using TV (upper) and NLTV (lower) models.

knowledge, these basic results are not found in the literature. Secondly, we study an objective function for image decomposition by consisting of the NLTV of the reflectance component, the H_1-norm of the illumination component, the data-fitting term between the input image, the reflectance and illumination components, and the L_2-norm of the illumination component. The first two terms have been employed in L_1-based Retinex [22]. The last term has been used in the Retinex methods [1, 2] for the fidelity term between reflectance and input image. Instead of using the equality constraint between the input image, the reflectance and illumination components, we measure their difference and employ it as a data-fitting term in the proposed model. In the paper, we provide the existence and uniqueness results of the NLTV model. We employ an alternating minimization algorithm to solve the NLTV model numerically. The convergence results of the minimization algorithm are also presented. Experimental results on both grey-level and color images are shown to illustrate the usefulness of the nonlocal total variation image decomposition model. The performance of the NLTV model is better than that of the other testing methods.

The paper is organized as follows. In Section 2, we present the theoretical results related to the space of nonlocal bounded variation functions. In Section 3, we study the proposed nonlocal decomposition model and the algorithm. In Section 4, we give the numerical examples. Finally, some concluding remarks are presented in Section 5.

2. Basic results

2.1. Space of bounded variation functions

The space of functions of bounded variation $(BV(\Omega))$ [25] is well adapted for the purpose of understanding the gradient of discontinuous functions. In this paper, we

assume Ω to be a bounded open subset of $\mathbb{R}^N$, and assume $u \in L^1(\Omega)$, we set,

$$\int_\Omega |Du| = \sup \left\{ \int_\Omega u(x)\mathrm{div}(\varphi(x))\mathrm{dx} \mid \varphi \in C_0^1(\Omega)^N, \ \|\varphi\|_{L^\infty} \leq 1 \right\},$$

where $\mathrm{div}\varphi = \sum_{i=1}^N \frac{\partial \varphi_i}{\partial x_i}$, dx is the Lebesgue measure, $C_0^1(\Omega)^N$ is the space of continuously differentiable functions with compact support in Ω, and $\|\varphi\|_{L^\infty} = \sup_x \sqrt{\sum_i \varphi_i^2}$. Then we define $BV(\Omega)$ as follows:

$$BV(\Omega) = \left\{ u \in L^1(\Omega); \ \int_\Omega |Du| < \infty \right\}.$$

There are several main properties of $BV(\Omega)$.

- Lower semicontinuity: Let $u_n \in BV(\Omega)$, and $u_n \xrightarrow[L^1(\Omega)]{} u$, then,

$$\liminf_{n \to +\infty} \int_\Omega |Du_n| \geq \int_\Omega |Du|.$$

- Approximation: Let $u \in BV(\Omega)$, there exists a sequence $\{u_n\} \subset C^\infty(\Omega) \bigcap BV(\Omega)$ satisfying $u_n \xrightarrow[L^1(\Omega)]{} u$, and,

$$\lim_{n \to +\infty} \int_\Omega |Du_n| = \int_\Omega |Du|.$$

- Compactness: Let $\{u_n\} \subset BV(\Omega)$ be uniformly bounded sequence, there exist a subsequence(still noted as $\{u_n\}$) and $u \in BV(\Omega)$, such that,

$$u_n \xrightarrow[L^1(\Omega)]{} u.$$

The success of the space of bounded variation functions comes from the fact that it allows discontinuous solutions. Hence the total variation regularization can be used in image processing models to preserve edges [26]. However, there are some limitations of total variation regularization. For instance, it cannot be used to preserve fine details and textures in image processing.

2.2. Space of nonlocal bounded variation functions

Recently, nonlocal regularization techniques are proposed and developed in [27–31]. Nonlocal regularizing functionals are formulated by Kindermann et al. in [32], and by Gilboa and Osher in [33, 34]. NLTV are proposed and used in many image processing applications, see for instance [35–37].

For $u \in W^{1,1}(\Omega)$, we define the nonlocal gradient as follows:

$$\nabla_{NL}u : \ \Omega \times \Omega \to \mathbb{R}^2, \quad (x,y) \mapsto (\nabla u(y) - \nabla u(x))\sqrt{\omega(x,y)},$$

where $\omega(x,y)$ satisfies,

$$\omega(x,y) \geq 0, \quad \omega(x,y) = \omega(y,x).$$

Assume $\mathbf{p}_1, \ \mathbf{p}_2 : \Omega \times \Omega \to \mathbb{R}^2$, we define the following nonlocal inner product of $\mathbf{p}_1, \ \mathbf{p}_2$,

$$\langle \mathbf{p}_1, \mathbf{p}_2 \rangle_{NL} = \int_{\Omega \times \Omega} \mathbf{p}_1(x,y) \cdot \mathbf{p}_2(x,y) \mathrm{dxdy},$$

where the dot product on the right hand side represents the dot product of $\mathbb{R}^2$. For any $\mathbf{p} : \Omega \times \Omega \to \mathbb{R}^2$, we can further define the nonlocal divergence and the nonlocal Laplacian as follows:

$$(\mathrm{div}_{NL}\mathbf{p})(x) = \int_\Omega (\mathrm{div}_x(\mathbf{p}(y,x)\sqrt{\omega(x,y)}) - \mathrm{div}_x(\mathbf{p}(x,y)\sqrt{\omega(x,y)}))\mathrm{dy},$$

$$(\Delta_{NL}u)(x) = \mathrm{div}_{NL}(\nabla_{NL}u)(x) = 2\int_\Omega (\omega(x,y)\Delta u(x) - \nabla_x\omega \cdot (\nabla u(y) - \nabla u(x)))\mathrm{dy}.$$

Now we establish the following properties for the above nonlocal operators.

Proposition 2.1. *Assume $u, \ v \in W^{1,1}(\Omega)$, $\mathbf{p}$ is differentiable, and $\omega(x,\cdot) \in C_0^1(\Omega)$, then the following equalities hold:*

$$\langle \nabla_{NL}u, \mathbf{p} \rangle_{NL} = -\langle u, \mathrm{div}_{NL}\mathbf{p} \rangle, \quad \langle \nabla_{NL}u, \nabla_{NL}v \rangle_{NL} = -\langle \Delta_{NL}u, v \rangle,$$

$$\langle \Delta_{NL}u, v \rangle = \langle u, \Delta_{NL}v \rangle, \qquad \int_\Omega (\mathrm{div}_{NL}\mathbf{p})(x)\mathrm{dx} = 0.$$

Proof. For the first equality, we have,

$$\langle \nabla_{NL}u, \mathbf{p} \rangle_{NL}$$

$$= \int_{\Omega \times \Omega} \sqrt{\omega(x,y)}((\nabla u(y) - \nabla u(x)) \cdot \mathbf{p}(x,y)\mathrm{dydx}$$

$$= \int_{\Omega \times \Omega} \nabla u(y) \cdot (\mathbf{p}(x,y)\sqrt{\omega(x,y)})\mathrm{dydx} - \int_{\Omega \times \Omega} \nabla u(x) \cdot (\mathbf{p}(x,y)\sqrt{\omega(x,y)})\mathrm{dxdy}$$

$$= -\int_\Omega \int_\Omega u(y)\mathrm{div}_y(\mathbf{p}(x,y)\sqrt{\omega(x,y)})\mathrm{dydx} + \int_\Omega \int_\Omega u(x)\mathrm{div}_x(\mathbf{p}(x,y)\sqrt{\omega(x,y)})\mathrm{dxdy}$$

$$= -\int_\Omega \int_\Omega u(x)\mathrm{div}_x(\mathbf{p}(y,x)\sqrt{\omega(x,y)})\mathrm{dxdy} + \int_\Omega \int_\Omega u(x)\mathrm{div}_x(\mathbf{p}(x,y)\sqrt{\omega(x,y)})\mathrm{dxdy}$$

$$= \int_{\Omega \times \Omega} u(x)(\mathrm{div}_x(\mathbf{p}(x,y)\sqrt{\omega(x,y)}) - \mathrm{div}_x(\mathbf{p}(y,x)\sqrt{\omega(x,y)}))\mathrm{dydx}$$

$$= -\int_\Omega u(x)(\int_\Omega (\mathrm{div}_x(\mathbf{p}(y,x)\sqrt{\omega(x,y)}) - \mathrm{div}_x(\mathbf{p}(x,y)\sqrt{\omega(x,y)}))\mathrm{dy})\mathrm{dx}$$

$$= -\langle u, \mathrm{div}_{NL}\mathbf{p} \rangle.$$

Then we have,

$$\langle \nabla_{NL} u, \nabla_{NL} v \rangle_{NL} = -\langle u, \mathrm{div}_{NL}(\nabla_{NL} v) \rangle = -\langle u, \Delta_{NL} v \rangle$$
$$= -\langle \mathrm{div}_{NL}(\nabla_{NL} u), v \rangle = -\langle \Delta_{NL} u, v \rangle,$$

$$\int_\Omega (\mathrm{div}_{NL}\mathbf{p})(x)\mathrm{dx} = \langle 1, \mathrm{div}_{NL}\mathbf{p} \rangle = -\langle \nabla_{NL} 1, \mathbf{p} \rangle_{NL} = 0.$$

This completes the proof. □

Next we generalize the nonlocal gradient as follows. Assume $u \in L^1(\Omega)$, and the nonlocal total variation NLTV is given by

$$NLTV(u) = \int_\Omega |D_{NL} u| = \sup_{\phi \in C_0^1(\Omega \times \Omega)^2, \|\phi\|_\infty \leq 1} \int_\Omega u(x)\mathrm{div}_{NL}\phi(x)\mathrm{dx}.$$

The corresponding set $NLBV(\Omega)$ of functions is given by,

$$NLBV(\Omega) = \{u \in L^1(\Omega), \ NLTV(u) < \infty\}.$$

Now we give some properties of $NLBV(\Omega)$ similar to that of $BV(\Omega)$.

Proposition 2.2 (Lower semicontinuity). *Let $u_n \in NLBV(\Omega)$, and $u_n \xrightarrow[L^1(\Omega)]{} u$, Then,*

$$\liminf_{n\to\infty} \int_\Omega |D_{NL} u_n| \geq \int_\Omega |D_{NL} u|.$$

Proof. For fixed $\phi \in C_0^1(\Omega \times \Omega)^2$, satisfying $\|\phi\|_\infty \leq 1$,

$$\int_\Omega u\mathrm{div}_{NL}\phi\mathrm{dx} = \lim_{n\to\infty} \int_\Omega u_n \mathrm{div}\phi\mathrm{dx} \leq \liminf_{n\to\infty} \int_\Omega |D_{NL} u_n|.$$

Taking supremum for ϕ, the result follows. □

Proposition 2.3 (Approximation). *For any $u \in NLBV(\Omega)$, There exist a sequence $\{u_n\} \subset NLBV(\Omega) \cap C^\infty(\Omega)$, such that,*

$$\lim_{n\to\infty} \int_\Omega |u_n - u|\mathrm{dx} = 0, \quad \lim_{n\to\infty} \int_\Omega |D_{NL} u_n| = \int_\Omega |D_{NL} u|.$$

Proof. As is shown in [25], we can find a sequence $u_\epsilon \in NLBV(\Omega) \cap C^\infty(\Omega)$ such that,

$$\int_\Omega |u_\epsilon - u|\mathrm{dx} \to 0, \quad \text{as} \ \ \epsilon \to 0.$$

For fixed $\phi \in C_0^\infty(\Omega \times \Omega)^2$, satisfying $\|\phi\|_\infty \leq 1$,

$$\int_\Omega u\mathrm{div}_{NL}\phi\mathrm{dx} = \lim_{\epsilon\to 0} \int_\Omega u_\epsilon \mathrm{div}_{NL}\phi\mathrm{dx}.$$

Therefore,

$$\lim_{\epsilon \to 0} \int_\Omega u_\epsilon \mathrm{div}_{NL}\phi \mathrm{dx} \leq \int_\Omega |D_{NL}u|.$$

According to the above equation, we can find $\epsilon_0 > 0$, such that if $\epsilon < \epsilon_0$,

$$\int_\Omega u_\epsilon \mathrm{div}_{NL}\phi \mathrm{dx} \leq \int_\Omega |D_{NL}u|.$$

Then for $\epsilon < \epsilon_0$,

$$\int_\Omega |D_{NL}u_\epsilon| \leq \int_\Omega |D_{NL}u|.$$

Noting the Lower semicontinuity, we have,

$$\int_\Omega |D_{NL}u| \leq \liminf_{\epsilon \to 0} \int_\Omega |D_{NL}u_\epsilon| \leq \limsup_{\epsilon \to 0} \int_\Omega |D_{NL}u_\epsilon| \leq \int_\Omega |D_{NL}u|.$$

This completes the proof. □

Proposition 2.4 (Compactness)**.** *Assume $\{u_n\}$ is uniformly bounded in $NLBV(\Omega)$, there exist a subsequence (still noting as $\{u_n\}$) and $u \in NLBV(\Omega)$, such that $u_n \xrightarrow[L^1(\Omega)]{} u$.*

Proof. By using Proposition 2.3, we can find a sequence $\{v_n\} \subset NLBV(\Omega) \cap C^\infty(\Omega)$ such that, for any positive integer k,

$$\| v_k - u_k \|_{L^1(\Omega)} \leq \frac{1}{k}, \quad \int_\Omega |D_{NL}v_k| \leq \int_\Omega |D_{NL}u_k| + \frac{1}{k}.$$

By using Lemma 5.3 in [38], there exist a constant $C(\Omega)$ such that,

$$\int_\Omega |\nabla v_k| \mathrm{dx} \leq C(\Omega) \bigg(\int_\Omega |\nabla_{NL}v_k| \mathrm{dx} + \| v_k \|_{L^1(\Omega)} \bigg).$$

Therefore, $\{v_n\}$ is uniformly bounded in $BV(\Omega)$. Noting the compactness of $BV(\Omega)$, there exist a subsequence (still noting as $\{u_n\}$) and $u \in BV(\Omega)$ such that $u_n \xrightarrow[L^1(\Omega)]{} u$.

In a word, We can find a subsequence $\{u_n\}$ corresponding to $\{v_n\}$ such that,

$$u_n \xrightarrow[L^1(\Omega)]{} u.$$

Noting the Lower semicontinuity,

$$\liminf_{i \to \infty} \int_\Omega |D_{NL}u_i| \geq \int_\Omega |D_{NL}u|.$$

Then we have $u \in NLBV(\Omega)$. □

   In the next section, we will use these theoretical results of the space of NLBV functions to study the existence of minimizer of NLTV energy functional.

3. The NLTV Retinex model

In the model, we assume that the intensity of an image S defined on the region Ω depends on two components. The first component is modeled as the amount of light intensity onto the objects in the image scene. The second component is the amount of light source reflected based on the nature of the objects in the image scene. In the formulation, we consider the intensity of an image is product of the illumination component U and the reflectance component R, i.e., $S = U \circ R$, where $\circ$ refers to the pointwise multiplication operation. The reflectance function is related to reflectivity of the objects, and therefore we impose the condition: $0 < R \leq 1$. The illumination function is related to illumination effect on the objects, and therefore we impose the condition: $0 < U < \infty$. The product form can be handled more effectively by considering the form in the domain of logarithm, i.e., $s = \log(S)$, $u = \log(U)$, $r' = \log(R)$. It is clear that we derive the following relation: $s = u + r'$. Because $0 < R \leq 1$, we obtain $r = -r' \geq 0$. It follows that the model becomes $u = s + r$.

In this paper, we employ the nonlocal total variation to represent the reflectance component. We study the following energy functional for image decomposition:

$$\Phi(r, u) = \int_\Omega |D_{NL}r| + \frac{c_1}{2}\int_\Omega |\nabla u|^2 \mathrm{dx} + \frac{c_2}{2}\int_\Omega (u - r - s)^2 \mathrm{dx} + \frac{c_3}{2}\int_\Omega u^2 \mathrm{dx}. \quad (3.1)$$

where c_i $(i = 1, 2, 3)$ are positive parameters to control the balance of different terms. Here we consider the spatially smoothness of the illumination component, and therefore the regularization term $\int_\Omega |\nabla u|^2$ can be used; the reflectance function is of nonlocal bounded variation, and therefore nonlocal total variation regularization $\int_\Omega |D_{NL}r|$ is used. The fitting term is given by $\int_\Omega (u - r - s)^2 \mathrm{dx}$. The term $\int_\Omega u^2 \mathrm{dx}$ has been used in [1, 2]. Also it can be used to establish the theoretical results [24].

In the following discussion, we consider the set:

$$\Lambda = \{(r, u) \mid (r, u) \in NLBV(\Omega) \times W^{1,2}(\Omega), \ r \geq 0, \ u \geq s\}.$$

The resulting optimization problem for the image decomposition is given by:

$$\min_{(r,u)\in\Lambda} \Phi(r, u). \quad (3.2)$$

Then we show that the solution of this optimization problem exists.

Theorem 3.1. *Let $s \in L^\infty(\Omega)$, then the problem* (3.2) *has a unique solution.*

Proof. The proof of the existence is similar to that of Theorem 2.1 in [24] by using Propositions 2.2 and 2.4. Moreover, we note that the Hessian of the last two terms in (3.1) is given by:

$$\begin{pmatrix} c_2 + c_3 & -c_2 \\ -c_2 & c_2 \end{pmatrix},$$

which is a positive definite matrix. As both the NLTV of r and H_1-norm of u are convex, it implies that the objective function in (3.1) is strictly convex. By noting that the

convexity of the constraint set, the uniqueness of the solution holds. The result follows.

$\square$

Next we present the alternating minimization scheme for solving problem (3.2).

Algorithm 3.1.

1. Take $k = 0$ and $u^0 = s$ be the initial guess of illumination component;

2. At the kth iteration:

   - Given u^k, compute $r^{k+\frac{1}{2}}$ by solving:

$$\min_r J_1(r) \equiv \int_\Omega |D_{NL}r| + \frac{c_2}{2} \int_\Omega (r + s - u^k)^2 \mathrm{dx}, \qquad (3.3)$$

   and update r^{k+1} by using:
$$r^{k+1} = \max\{r^{k+\frac{1}{2}}, 0\}; \qquad (3.4)$$

   - Given r^{k+1}, compute $u^{k+\frac{1}{2}}$ by solving:

$$\min_u J_2(u) \equiv \frac{c_1}{2} \int_\Omega |\nabla u|^2 \mathrm{dx} + \frac{c_2}{2} \int_\Omega (u - r^{k+1} - s)^2 \mathrm{dx} + \frac{c_3}{2} \int_\Omega u^2 \mathrm{dx}, \qquad (3.5)$$

   and update u^{k+1} by using:
$$u^{k+1} = \max\{u^{k+\frac{1}{2}}, s\}; \qquad (3.6)$$

3. Goto Step (2) until $\frac{||u^{k+1}-u^k||}{||u^{k+1}||} \leq \epsilon_u$ and $\frac{||r^{k+1}-r^k||}{||r^{k+1}||} \leq \epsilon_r$.

For the given optimization subproblem in (3.3), we employ the Split Bregman method which is introduced in [39], and extended to a nonlocal version in [37] to solve it.

For the given optimization subproblem in (3.5), we can obtain the solution by using fast Fourier transform:

$$u^{k+1} = \mathcal{F}^{-1}\left(\frac{c_2 \mathcal{F}(r^{k+1} + s)}{c_1(\mathcal{F}^*(\nabla_x)\mathcal{F}(\nabla_x) + \mathcal{F}^*(\nabla_y)\mathcal{F}(\nabla_y)) + c_2 + c_3}\right).$$

Below we present two theorems to demonstrate the projections in (3.4) and (3.6) can give their associated solutions of the two given optimization subproblems.

Theorem 3.2. *Let* $\Psi = \{r : r \in NLBV(\Omega), r \geq 0\}$. *If* $\hat{r_*}$ *is the solution of the optimization problem in* (3.3), *then* $\hat{r} = \max\{\hat{r_*}, 0\}$ *as in* (3.4) *is the solution of the optimization problem as follows:*

$$\min_{r \in \Psi} J_1(r).$$

Theorem 3.3. *Let* $\Xi = \{u : u \in W^{1,2}(\Omega), u \geq s\}$. *If* $\hat{u_*}$ *is the solution of the optimization problem in* (3.5), *then* $\hat{u} = \max\{\hat{u_*}, s\}$ *is the solution of the optimization problem as follows:*

$$\min_{u \in \Xi} J_2(u).$$

We remark that the proofs of Theorems 3.3 and 3.4 are similar to that in Theorem 3.3 [24] by using Propositions 2.2 and 2.3.

Now we can establish the convergence of Algorithm 3.1.

Theorem 3.4. *Let $\{(r^k, u^k)\}$ be the sequence generated by Algorithm 3.1. Then $\{(r^k, u^k)\}$ converges to $(r_*, u_*) \in \Lambda$ (up to a subsequence in the convergence), which is the unique solution of problem in (3.2).*

Proof. As the proof of Theorem 3.5 in [24], we derive the similar result by using Propositions 2.2 and 2.4, i.e., assume that $\{(r^k, u^k)\}$ is the sequence generated by Algorithm 3.1, then $\{(r^k, u^k)\}$ converges to $(r_*, u_*) \in \Lambda$ (up to a subsequence in the convergence), and we have for any $r \in \Psi$ and $u \in \Xi$,

$$\Phi(r_*, u_*) \leq \Phi(r, u_*), \quad \Phi(r_*, u_*) \leq \Phi(r_*, u).$$

According to the optimality condition of each subproblem in Algorithm 3.1, we have

$$0 \in \partial J_{NL}(r_*) + c_2(r_* + s - u_*), \tag{3.7}$$

and

$$0 \in \frac{c_1}{2}\partial J(u_*) + c_2(u_* - r_* - s) + c_3 u^*, \tag{3.8}$$

where $J_{NL}(r)$ and $J(u)$ refers to $\int_\Omega |D_{NL}r|$ and $\int_\Omega |\nabla u|^2 dx$ respectively. The subdifferential of $\Phi(r, u)$ at (r_*, u_*) is given by

$$\partial\Phi(r_*, u_*) = \partial\left(\int_\Omega |D_{NL}r_*| + \frac{c_1}{2}\int_\Omega |\nabla u_*|^2 dx + \frac{c_2}{2}\int_\Omega (u_* - r_* - s)^2 dx + \frac{c_3}{2}\int_\Omega u_*^2 dx\right)$$

$$= \partial\left(J_{NL}(r_*) + \frac{c_1}{2}J(u_*)\right) + \partial\left(\frac{c_2}{2}\int_\Omega (u_* - r_* - s)^2 dx + \frac{c_3}{2}\int_\Omega u_*^2 dx\right).$$

Noting that the part $\frac{c_2}{2}\int_\Omega (u - r - s)^2 dx + \frac{c_3}{2}\int_\Omega (u)^2 dx$ is differentiable at (r_*, u_*), we have

$$\partial\left(\frac{c_2}{2}\int_\Omega (u_* - r_* - s)^2 dx + \frac{c_3}{2}\int_\Omega u_*^2 dx\right) = \begin{pmatrix} c_2(r_* + s - u_*) \\ c_2(u_* - r_* - s) + c_3 u_* \end{pmatrix}. \tag{3.9}$$

Since $J(u)$ is continuous, we have,

$$\partial\left(J_{NL}(r_*) + \frac{c_1}{2}J(u_*)\right) = \begin{pmatrix} \partial J_{NL}(r_*) \\ \frac{c_1}{2}\partial J(u_*) \end{pmatrix}. \tag{3.10}$$

Therefore,

$$\partial\Phi(r_*, u_*) = \begin{pmatrix} \partial J_{NL}(r_*) + c_2(r_* + s - u_*) \\ \frac{c_1}{2}\partial J(u_*) + c_2(u_* - r_* - s) + c_3 u_* \end{pmatrix}.$$

By combining the above equation with (3.7) and (3.8), we derive

$$\begin{pmatrix} 0 \\ 0 \end{pmatrix} \in \partial\Phi(r_*, u_*).$$

It is equivalent that (r_*, u_*) is the solution of the problem (3.2). This completes the proof. □

4. Numerical results

In this section, we test Algorithm 3.1 on several images to illustrate the effectiveness of the proposed model. In Algorithm 3.1, we set the stopping criteria to be $\epsilon_u = \epsilon_r = 1 \times 10^{-4}$. Also we use nonlocal weight ω with patch size 5×5, ten best neighbors in the searching window of 11×11, which has been introduced in [37], and we update the weight iteratively along with steps (3.3)-(3.6). When we deal with color images, we perform the proposed model in HSV color space. More precisely, we apply Algorithm 3.1 to the V channel of HSV color space to obtain the illumination and reflectance components. Similar to [5], we consider to use a corrected version of the computed illumination. The procedure computes the illumination image $U = \exp(u)$ and the reflectance image $R = \exp(-r)$ from Algorithm 3.1. The Gamma correction of U with an adjusting parameter γ is defined by:

$$U' = W \left(\frac{U}{W} \right)^{\frac{1}{\gamma}}.$$

We remark that W refers to the white value which is equal to 255 in a 8-bit image. The final result is then given by:

$$S' = U' \cdot R.$$

For color images, the resulting V-channel image and the other original H and S channels provide the final enhanced image. In Fig. 2(d), we see the picture without using the Gamma correction is over-enhanced. In Fig. 2(e), we see the picture without using Retinex decomposition but with Gamma correction only, the resulting image cannot be enhanced. However, the pictures in Figs. 2(b) and 2(c) with using both Retinex decomposition and the Gamma correction are visually more natural.

4.1. The effect of parameters for recovered reflectance

In the first test, we demonstrate the effect of the parameter in the Gamma correction procedure. In Fig. 3, we show the results of enhanced images by using different values of γ: $2.2, 10, 100, 1000$. We see from the figure that the enhanced images by using TV Retinex model are not sharp and pleasant enough. In particular, when γ is large, some information like in the wall paintings are lost. However, the enhanced images by using the proposed NLTV Retinex model are visually appealing, and the proposed method is more robust for different values of γ.

In the next test, we study the effect of parameters c_1, c_2, and c_3. First we set $c_2 = 1, c_3 = 10^{-5}$, and $c_1 = 0.01, 0.1, 1, 10$. Recall that c_1 controls the contribution of the regularization term of the illumination function. We see from the first row of Fig. 4 that the reflectance component becomes flatter as c_1 decreases. Then we set $c_1 = 1, c_3 = 10^{-5}$, and $c_2 = 0.01, 0.1, 1, 10$, and we see from the second row of Fig. 4 that the reflectance component is enhanced gradually as c_2 increases. Finally, we set $c_1 = 1, c_2 = 1$, and $c_3 = 10^{-2}, 10^{-3}, 10^{-4}, 10^{-5}$. As is show in the third row of Fig. 4,
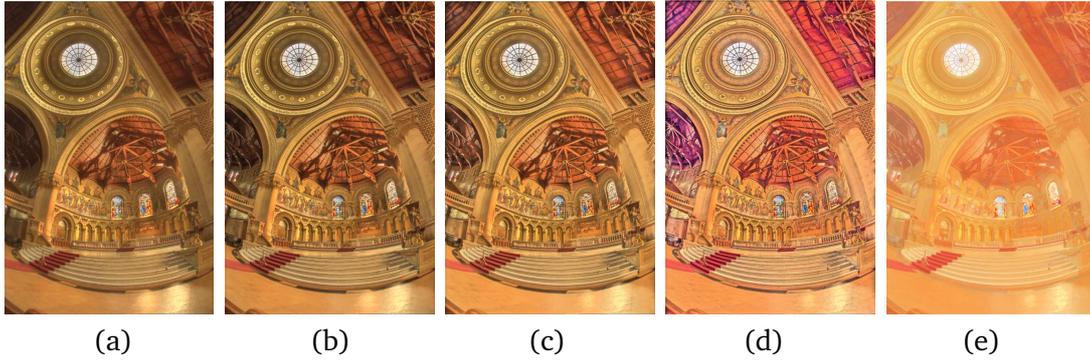
Figure 2: (a) The input image; the resulting images using both Retinex decomposition and Gamma correction: (b) $[\gamma = 2.2]$ and (c) $[\gamma = 10]$; (d) the resulting image using Retinex decomposition without Gamma correction; (e) the resulting image without using Retinex decomposition but with Gamma correction $[\gamma = 10]$. Here the parameters are set: $c_1 = 1$, $c_2 = 1$ and $c_3 = 10^{-5}$.
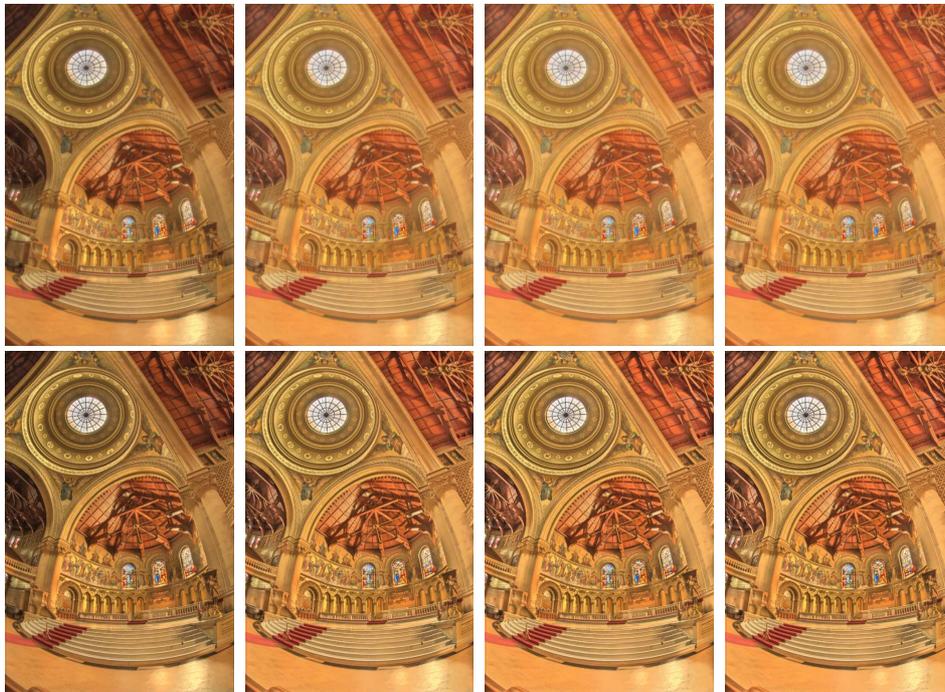

Figure 3: The first row: the enhanced images by TV Retinex model with $\gamma = 2.2, 10, 100, 1000$ respectively; the second row: the enhanced images by NLTV Retinex model with $\gamma = 2.2, 10, 100, 1000$ respectively.

the reflectance component is over-enhanced with $c_3 = 10^{-2}$, and other results change very little as c_3 varies. Similarly, we show in Fig. 5 the illumination components for the above sets of parameters. We see from the first row and the second row of Fig. 5 that the illumination component turns sharper as c_1 decreases, and the illumination component is less smoothed as c_2 increases. We see from the third row of Fig. 5 that the
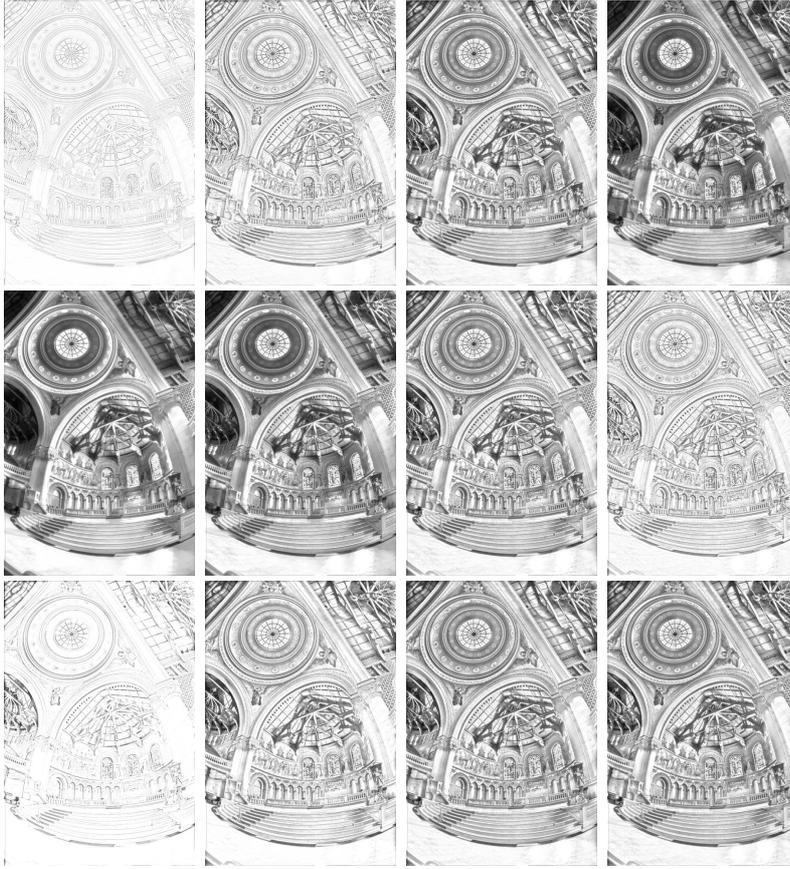
Figure 4: The first row: the reflectance component by using the proposed model with $c_2 = 1, c_3 = 10^{-5}$, and $c_1 = 0.01, 0.1, 1, 10$ respectively; the second row: the reflectance component by using the proposed model with $c_1 = 1, c_3 = 10^{-5}$, and $c_2 = 0.01, 0.1, 1, 10$ respectively; the third row: the reflectance component by using the proposed model with $c_1 = 1, c_2 = 1$, and $c_3 = 10^{-2}, 10^{-3}, 10^{-4}, 10^{-5}$ respectively.

illumination component is weakened with $c_3 = 10^{-2}$, and again other results change very little as c_3 varies.

In the following experiments, we fix $\gamma = 2.2$, $c_1 = c_2 = 1$ and $c_3 = 10^{-5}$ in the proposed NLTV Retinex model to test its performance.

4.2. Enhanced images by different methods

In this subsection, we compare the results of NLTV model with Kimmel's method in [5], L_1-based method in [22], nonlocal method in [21] and TV Retinex model in [24]. We use the parameters in the tests: $\alpha = 0.0001$ and $\beta = 0.1$ in [5], $t = 10$ in [22], $t = 10$ in [21], and $\alpha = 1$, $\beta = 1$, $\mu = 10^{-5}$ in TV Retinex model [24]. These parameters are fixed as that in [5,21,22,24] to generate good enhanced images visually with respect to different methods. We remark that the computational times of one iteration in Kimmel's
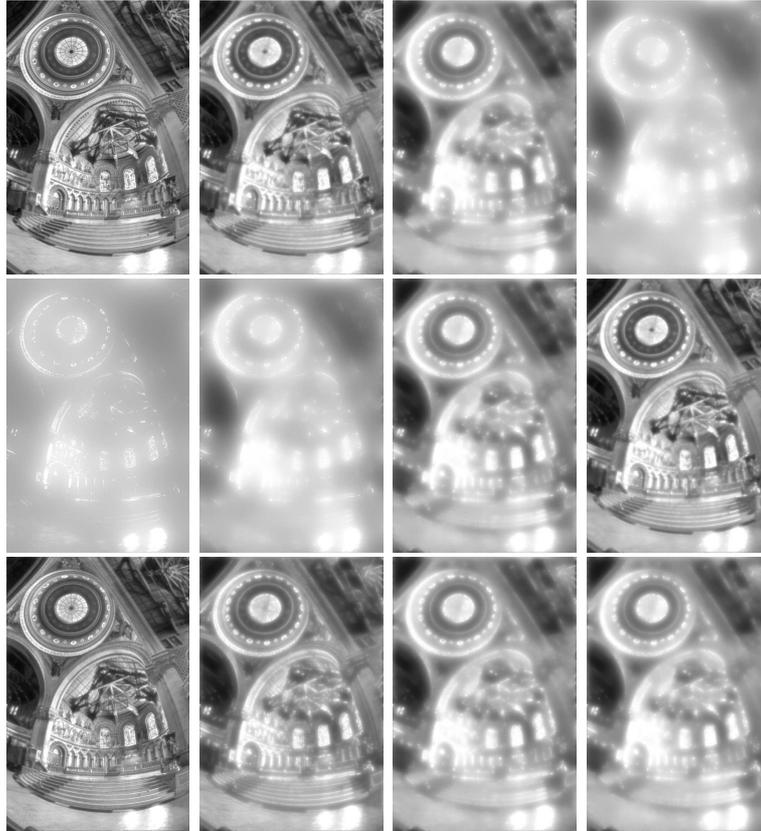
Figure 5: The first row: the illumination component by using the proposed model with $c_2 = 1, c_3 = 10^{-5}$, and $c_1 = 0.01, 0.1, 1, 10$ respectively; the second row: the illumination component by using the proposed model with $c_1 = 1, c_3 = 10^{-5}$, and $c_2 = 0.01, 0.1, 1, 10$ respectively; the third row: the illumination component by using the proposed model with $c_1 = 1, c_2 = 1$, and $c_3 = 10^{-2}, 10^{-3}, 10^{-4}, 10^{-5}$ respectively.

method, L_1-based method, TV Retinex model in [24], nonlocal method in [21], and the proposed NLTV model are 1.32, 0.58, 0.49, 5.48, and 5.54 seconds, respectively for an 512×768 image. We note in the last two methods that nonlocal weights are required to handle in each iteration. Therefore, more computational time is needed.

In Fig. 6, we show five input underexposed images for enhancement. We give the enhancement results in Figs. 7(a), 7(b) and 7(c), 7(d) and 7(e), 7(f), 7(g) correspond-ing to Kimmel's method [5], L_1-based method [22], nonlocal method [21], TV Retinex model [24] and the proposed NLTV model. In [21, 22], their computed results are performed in RGB color space. As for a comparison, we show their results by using both RGB and HSV color spaces. Both the TV and NLTV models are performed in HSV color space‡. The visual quality of enhanced images in Figs. 7(c) and 7(e) under the

---

‡In our experiments, we find that the performance of the proposed NLTV method in HSV color space is better than that in RGB color space. Therefore we only display the enhancement results in the HSV color space.

Figure 6: Input images.

| (a) | (b) | (c) | (d) | (e) | (f) | (g) |

Figure 7: The enhanced images by using (a) Kimmel's method [5]; (b) L_1-based method [22] ($t = 10$) in HSV color space; (c) L_1-based method [22] ($t = 10$) in RGB color space; (d) nonlocal based method [21] ($t = 10$) in HSV color space;(e) nonlocal based method [21] ($t = 10$) in RGB color space; (f) TV Retinex [24] and (g) the proposed NLTV Retinex.

RGB color space are not good, especially in the second and third pictures. We see from Figs. 7(a) and 7(f) that the input images are enhanced uniformly in the whole image domain by Kimmel's method and TV Retinex model. We also observe that the nonlocal method in [21] preserve more details than the L_1-based method [22], but there are still some unpleasant distortions such as the region near the foot of the woman in the second image, and the sky part in the fifth image. The visual quality of the enhanced
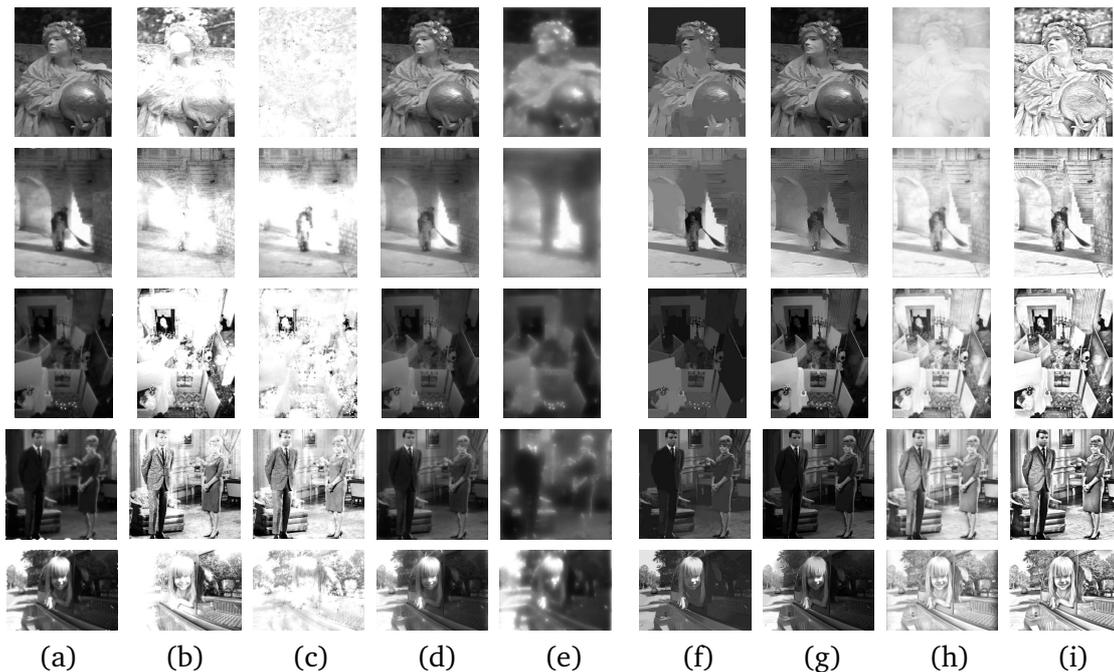
Figure 8: The illumination components by using (a) Kimmel's method [5], (b) L_1-based method [22], (c) nonlocal method [21], (d) TV Retinex [24], and (e) the proposed NLTV Retinex; The reflectance components by using (f) L_1-based method [22], (g) nonlocal method [21], (h) TV Retinex [24], and (i) the proposed NLTV Retinex.

images by the proposed NLTV Retinex model is better than that by the other testing methods. The output enhanced images are more sharper and clearer than those by the other testing methods. For instance, we see that the steps in the second image, the floor in the third image, and the sofa in the fourth image are clearly enhanced.

Moreover, we give the results of the recovered illumination components decomposed from Kimmel's method, L_1-based method, nonlocal method, TV Retinex and the proposed NLTV Retinex in Figs. 8(a), 8(b), 8(c), 8(d), and 8(e) respectively. We see from the results that the illumination components by NLTV Retinex model are smoother than those by other methods. In Figs. 8(f), 8(g), 8(h), and 8(i), we give the results of the reflectance components decomposed from L_1-based method, nonlocal method, TV Retinex and the proposed NLTV Retinex respectively. Again we see from the results that the reflectance components by using the proposed NLTV Retinex are sharper and clearer than those generated by the other methods.

Also we test the medical images in Fig. 9(a), and compare the proposed model with homomorphic filtering, Kimmel's method in [5], N3 method in [40], L_1-based method in [22], nonlocal method in [21] and TV Retinex model in [24] as well. Here N3 is not based on Retinex theory. It is a nonparametric method for automatic correction of intensity non-uniformity in medical images. We display the results by using homomorphic filtering, Kimmel's method in [5], N3 method in [40], L_1-based method

<div align="center">(a)   (b)   (c)   (d)   (e)   (f)   (g)   (h)</div>
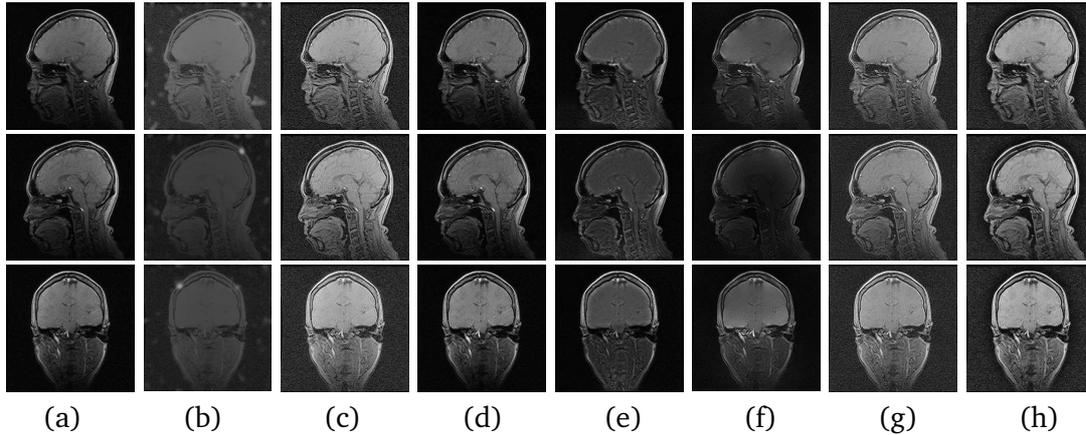
Figure 9: (a) the original images; (b) the enhanced results by using homomorphic filtering; (c)the enhanced results by using Kimmel's method [5]; (d) the enhanced results by using N3 method; (e) the enhanced results by using L_1-based method [22]($t = 2$); (f) the enhanced results by using nonlocal method [21]($t = 5$); (g) the enhanced results by using TV Retinex [24]; (h) the enhanced results by using the proposed NLTV Retinex model.

in [22], nonlocal method in [21], TV Retinex in [24] and the proposed NLTV Retinex model in Figs. 9(b), 9(c), 9(d), 9(e), 9(f), 9(g), and 9(h) respectively. We can see more details from the results by using the proposed model than those by using other methods. In particular, the results by using Kimmel's method, N3 method, L_1-based method, nonlocal method and TV Retinex lose some details in the brain. However, the proposed model can generate better enhanced images with high contrast and preserve more features in the enhancement.

4.3. Comparison by S-CIELAB color metric

In this test, we give a comparison by using the S-CIELAB color metric [41] which is very efficient for measuring color reproduction errors of digital images. The S-CIELAB color metric extends CIELAB by incorporating factors related to the pattern-color sensitivities of the human eye. The original image is shown in Fig. 11(a) with high contrast. We make use of Fig. 11(a) to generate twelve dark images by scaling of the pixel values. More precisely, the original image is divided into two parts with different scaling parameters to generate a nonuniform darkness. The corresponding scaling parameters in the two parts are set to be $(0.45, 0.40)$, $(0.50, 0.45)$, $(0.55, 0.50)$, $(0.60, 0.55)$, $(0.65, 0.60)$, $(0.70, 0.65)$, $(0.75, 0.70)$, $(0.80, 0.75)$, $(0.85, 0.80)$, $(0.90, 0.85)$, $(0.95, 0.90)$, $(1, 0.95)$ respectively. In Fig. 10, we show the S-CIELAB errors between the original image and the enhanced twelve images by using Kimmel's method in [5], TV Retinex in [24], and the proposed NLTV Retinex model. The pixel numbers whose S-CIELAB errors are larger than 5 units are considered. We can see from the results that the proposed NLTV Retinex model can produce better color restoration.

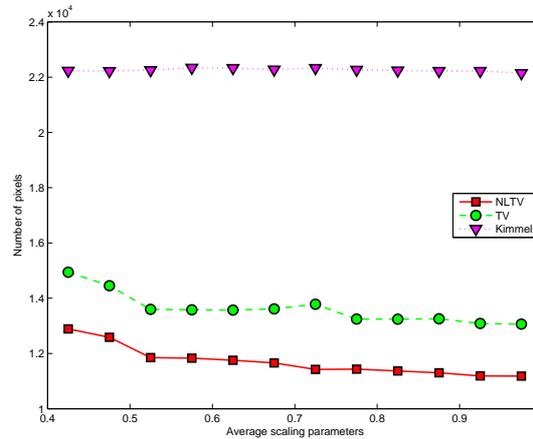As an example, we show a generated dark image in Fig. 11(b) with the scaling pa-

Figure 10: The S-CIELAB error that are 5 units or higher between the enhanced image and the original image. The x-axis refers to the twelve generated images.

rameter $(0.75, 0.70)$. The enhanced images are given in Figs. 11(c), 11(d), and 11(e) corresponding to Kimmel's method in [5], TV Retinex in [24] and the proposed NLTV Retinex, Figs. 11(f), 11(g), and 11(h) are the corresponding residuals in the V channel between the enhanced images and the original image. We see that the residual image by using Kimmel's method has the strongest contrast, i.e., the effect of the color restoration is the worst. The residual image by using TV Retinex model has lower contrast, however, some details like textures are involved. Therefore, we observe that the proposed NLTV Retinex model can produce best restoration results because NLTV regularization is able to preserve more detailed information. We further show the spatial distributions of S-CIELAB errors which are larger than 5 units between Fig. 11(a) and Figs. 11(c), 11(d), and 11(e) in Figs. 11(i), 11(j), and 11(k) respectively. The corresponding histogram distribution of S-CIELAB errors gives the numbers of pixels per error unit, and are displayed in Figs. 11(l)-11(n). In this comparison, we find that there are about 13.96%, 8.61%, and 7.14% of image pixels whose S-CIELAB errors exceeding 5 units by using Kimmel's method, TV Retinex and the proposed NLTV Retinex. Because of the assumption that both illumination and reflectance components vary smoothly in Kimmel's method, there are 4159 image pixels whose errors are even larger than 25 units. In contrast, TV Retinex and NLTV Retinex only have 1885 and 312 image pixels whose errors are larger than 25 units. It is clear that there are more pixels in the range $[0, 5]$ of the S-CIELAB errors in Fig. 11(n). These results suggest that the proposed NLTV Retinex model can provide a good quality of enhanced images.

5. Conclusions

In this paper, we have presented to use nonlocal bounded variation (NLBV) techniques for Retinex to decompose an image intensity into illumination and reflectance
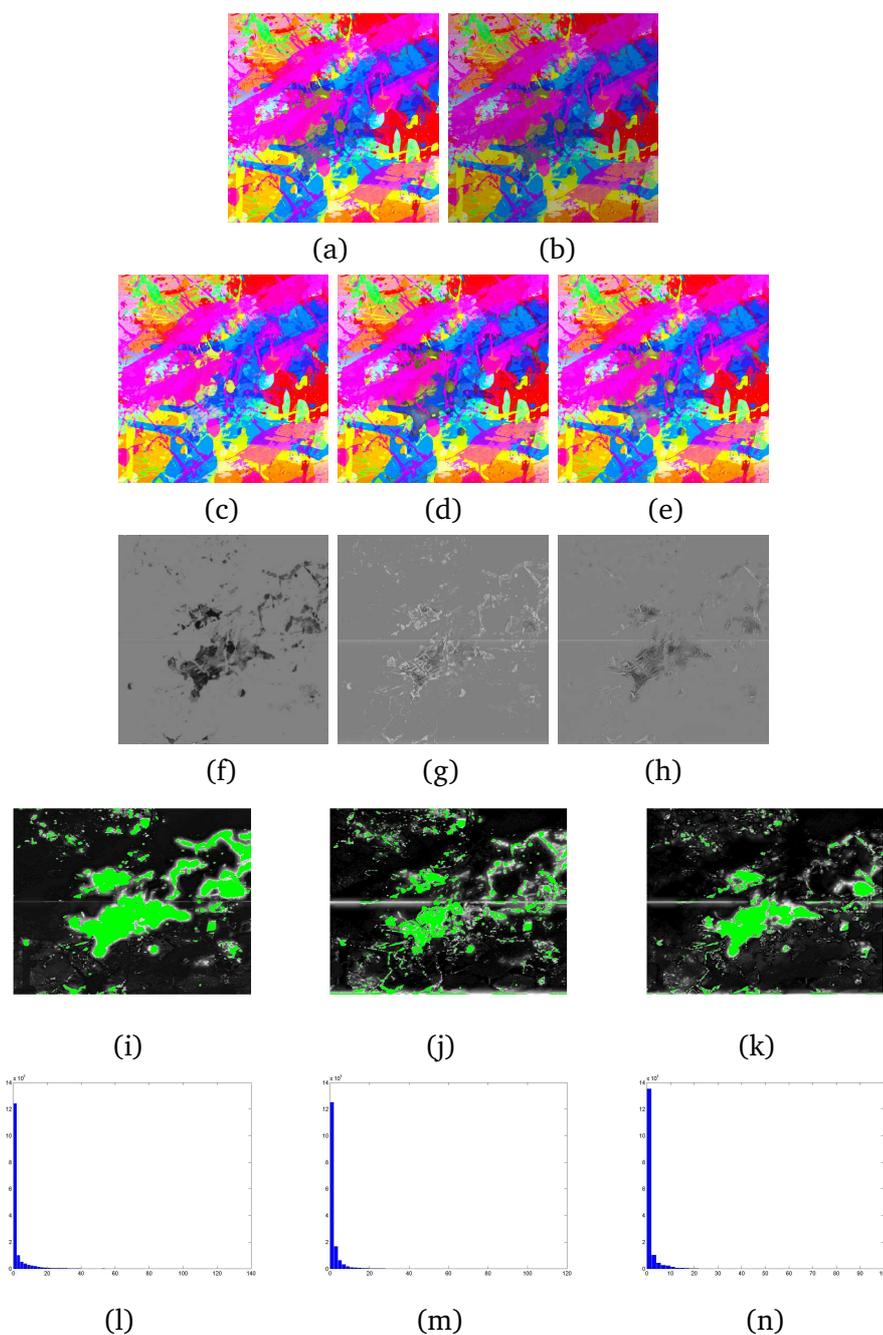
Figure 11: (a) The original image; (b) the dark input image; (c) the enhanced image by using Kimmel's method [5]; (d) the enhanced image by using TV Retinex [24]; (e) the enhanced image by using the proposed NLTV Retinex model; (f)-(h) the corresponding residual parts between (a) and (c), (d), (e); (i)-(k) the spatial distribution of the errors between Fig. (a) and Figs. (c), (d), (e) that are 5 units or higher (marked by green color); (l)-(n) the histogram distribution of S-CIELAB error between Fig. (a) and Figs. (c), (d), (e).

components. NLBV function space has been studied in the first part of this paper. We have given and proved some important properties of NLBV functions which are helpful to construct the minimization theory of the proposed NLTV Retinex model. We have shown the existence and uniqueness for the solution of the proposed model in the paper. We employed a fast computation method to solve the proposed minimization problem including the convergence results. Experimental results have been given to illustrate the effectiveness of the proposed model in terms of the quality of enhanced images.

In (3.1), the spatially smoothness assumption of the illumination component is considered, and the regularization term $\int_\Omega |\nabla u|^2$ is used. For the future research topic, we consider in (3.1) to use the L_1-norm of the gradient to handle images with shadows in the illumination component.

References

[1] M. Bertalmío, V. Caselles, and E. Provenzi, *"Issues about Retinex Theory and Contrast Enhancement,"* Int. J. Comput. Vis., vol. 83, no. 1, pp. 101-119, 2009.

[2] R. Palma-Amestoy, E. Provenzi, M. Bertalmío, and V. Caselles, *"A Perceptually Inspired Variational Framework for Color Enhancement,"* IEEE Trans. Pattern Anal. Mach. Intell., vol. 31, no. 3, pp. 458-474, 2009.

[3] B. Funt, M. Drew, and M. Brockington, *"Recovering shading from color images,"* in Lecture Notes in Computer Science: Computer Vision, ECCV92, vol. 588 G. Sandini, Ed. Berlin, Germany: Springer-Verlag, 1992, pp. 124132.

[4] N. Limare, J. M. Morel, A. Petro and C. Sbert, *"Retinex Poisson Equation: a Model for Color Perception,"* Image Processing On Line, 2011. http://dx.doi.org/10.5201/ipol.2011.lmps_rpe.

[5] R. Kimmel, D. Shaked, M. Elad, R. Keshet, and I. Sobel, *"A Variational Framework for Retinex,"* International Journal of Computer Vision, vol. 52, pp. 7-23, 2004.

[6] E. H. Land, and J. J. McCann, *"Lightness and Retinex Theory,"* J. Opt. Soc. Am., vol. 61, pp. 1-11, 1971.

[7] J. J. McCann, C Parraman and A. Rizzi, *"Pixel and Spatial Mechanisms of Color Constancy,"* IS&T/SPIE Electronic Imaging 2010, San Jose (California, USA), 17-21, January 2010.

[8] E. H. Land, *"The Retinex Theory of Color Vision,"* Sci. Amer., vol. 237, pp. 108-128, 1977.

[9] E. H. Land, *"Recent Advances in the Retinex Theory and Some Implications for Cortical Computations: Color Vision and Natural Image,"* proc. Nat. Acad. Sci. USA, vol. 80, pp. 5163-5169, 1983.

[10] J. Frankle and J. McCann, *"Method and Apparatus for Lightness Imaging,"* U.S. Patent 4384336, May 17, 1983.

[11] J. McCann, *"Lesson Learned from Mondrians Applied to Real Images and Color Gamuts,"* in Proc. IST/SID 7th Color Imag. Conf., pp. 1-8, 1999.

[12] B. Funt, F. Ciurea, and J. McCann, *"Retinex in Matlab,"* J. Electron. Imag., vol. 13, no. 1, pp. 48-57, 2004.

[13] J. J. McCann, and I. Sobel, *"Experiments with Retinex,"* HPL Color Summit, 1998.

[14] M. Bertalmío and J. Cowan, *"Implementing the Retinex Algorithm with Wilson-Cowan Equations,"* J. Physiol., vol. 103, pp. 69-72, 2009.

[15] B. K. P. Horn, *"Determining Lightness from an Image,"* Computer Graphics and Image Processing, vol. 3, pp. 277-299, 1974.

[16] A. Blake, *"Boundary Conditions of Lightness Computation in Mondrain World,"* Computer Vision Graphics and Image Processing, vol. 32, pp. 314-327, 1985.

[17] D. Terzopoulos, *"Image Analysis Using Multigrid Relaxation method,"* IEEE Trans. on PAMI, vol. 8, pp. 129-139, 1986.

[18] J. M. Morel, A. B. Petro, and C. Sbert, *"Fast Implementation of Color Constancy Algorithms,"* Proc. SPIE, vol. 7241, 724106, 2009. DOI:10.1117/12.805474.

[19] J. M. Morel, A. B. Petro, and C. Sbert, *"A PDE Formalization of Retinex Theory,"* IEEE Transactions on Image Processing, vol. 19, no. 11, pp. 2825-2837, 2010.

[20] Michael Elad, *"Retinex by Two Bilateral Filters,"* Scale Space and PDE Methods in Computer Vision, vol. 3459, pp. 217-229, 2005.

[21] W. Ma, and S. Osher, *"A TV Bregman Iterative Model of Retinex Theory,"* Inverse Problems and Imaging, vol. 6, No. 4, pp. 697-708, 2012.

[22] W. Ma, J. M. Morel, S. Osher and A. Chien, *"An L_1-based Variational Model for Retinex Theory and Its Applications to Medical Images,"* Computer Vision and Pattern Recognition (CVPR), IEEE Conference on., pp. 153-160, 2011.

[23] D. Zosso, G. Tran, and S. Osher, *"A unifying Retinex model based on non-local differential operators,"* Proc. SPIE 8657, Computational Imaging XI, 865702, 2013.

[24] M. Ng and W. Wang, *"A total variation model for Retinex,"* SIAM Journal on Imaging Sciences, vol. 4, no. 1, pp. 345-365, 2011.

[25] L. Ambrosio, N. Fusco, and D. Pallara, *"Functions of Bounded Variation and Free Discontinuity Problems,"* Oxford Mathematical Monographs. Oxford University Press, March 2000.

[26] L. Rudin, S. Osher, and E. Fatemi, *"Nonlinear total variation based noise removal algorithms,"* Physica D, vol. 60, pp. 259-268, 1992.

[27] L. P. Yaroslavsky, *"Digital picture processing,"* An introduction., Springer Verlag, 1985.

[28] S. M. Smith and J. M. Brady, *"SUSAN-a new approach to low level image processing,"* Int. Journal of Computer Vision, vol. 23, pp. 45-78, 1997.

[29] C. Tomasi and R. Manduchi, *"Bilateral filtering for gray and color images,"* in ICCV, Bombay, pp. 839-846, 1998.

[30] A. Buades, B. Coll, J. M. Morel, and C. Sbert, *"Non local demosaicing,"* In: Proceedings of the 2008 International Workshop on Local and Non-Local Approximation in Image Processing (LNLA08). Lausanne, Suisse.

[31] M. Protter, M. Elad, H. Takeda, P. Milanfar, *"Generalizing the Non-Local-Means to super-resolution reconstruction,"* IEEE TIP, vol. 18, no. 1, pp. 36-51, 2009.

[32] S. Kindermann, S. Osher, and P. W. Jones, *"Deblurring and denoising of images by nonlocal functionals,"* SIAM MMS, vol. 4, no. 4, pp. 1091-1115, 2005.

[33] G. Gilboa, and S. Osher, *"Nonlocal linear image regularization and supervised segmentation,"* SIAM MMS, vol. 6, no. 2, pp. 595-630, 2007.

[34] G. Gilboa, and S. Osher, *"Nonlocal operators with applications to image processing,"* SIAM MMS, vol. 7, no. 3, pp. 1005-1028, 2008.

[35] Y. Lou, X. Zhang, S. Osher, and A. Bertozzi, *"Image recovery via nonlocal operators,"* Journal of Scientific Computing, vol. 42, pp. 185-197, 2010.

[36] G. Peyré, S. Bougleux, and L. Cohen, *"Non-local regularization of inverse problems,"* ECCV, Part III, LNCS 5304: 57-68, 2008.

[37] X. Zhang, M. Burger, X. Bresson, and S. Osher, *"Bregmanized Nonlocal Regularization for Deconvolution and Sparse Reconstruction,"* SIAM J. Imaging Sci., vol. 3, no. 3, pp. 253-276, 2010.

[38] S. Kindermann, S. Osher and P. Jones, *"Deblurring and denoising of images by nonlocal functionals,"* SIAM Mutiscale Modeling and Simulation, vol. 4, no. 4, pp. 1091-1115, 2005.

[39] T. Goldstein and S. Osher, *"The Split Bregman Method for L1-Regularized Problems,"* SIAM Journal on Imaging Sciences, vol. 2, No. 2, PP. 323-343, 2009.

[40] J. G. Sled, A. P. Zijdenbos, and A. C. Evans, *"A nonparametric method for automatic correction of intensity nonuniformity in MRI data,"* IEEE Transactions on Medical Imaging, vol. 17, no. 1, pp. 87-97, 1998.

[41] X. Zhang and B. A. Wandell, *"A Spatial Extension of CIELAB for Digital Color Image Reproduction,"* SID Digest, pp. 731-734, 1996.